

A priori tests of one-equation LES modeling of rotating turbulence

HAO LU[†], CHRISTOPHER J. RUTLAND[‡] and LESLIE M. SMITH[§]

^{†, ‡}Engine Research Center, Department of Mechanical Engineering,
University of Wisconsin—Madison, WS, USA

[§]Departments of Mathematics and Engineering Physics, University of Wisconsin—Madison, WS, USA

A priori tests of subgrid-scale (SGS) models are performed using results of 128^3 direct numerical simulations for forced isotropic ($Re_\lambda = 100$) and rotating turbulence ($0.1 < Ro^{\omega 3} < 0.4$). A range of SGS models is tested varying from algebraic, gradient, and scale similarity, to one-equation viscosity and non-viscosity dynamic structure models. Anisotropy and material frame indifference (MFI) requirements for SGS models in rotating systems are reviewed and used to help construct new models based on the dynamic structure approach. The models are evaluated primarily using correlation and regression coefficients of individual components of the SGS tensor, components of the divergence of the SGS stresses, and the kinetic energy transfer term between large and small scales. For all measures examined, the MFI-consistent dynamic structure models perform significantly better, especially for rotating turbulence.

1. Introduction

Large eddy simulation (LES) of rotating turbulence is of interest because turbulent flows subject to solid-body rotation have a wide range of application in engineering science, geophysics and astrophysics. They also provide a simple configuration to study characteristic features and model performances in homogeneous but anisotropic turbulent flows.

The capability of subgrid-scale (SGS) models can be determined by comparing the predicted results with direct numerical simulation (DNS) or experimental data. Clark et al. [14], McMillan et al. [34] and Bardina et al. [1] are early examples of such studies. For such analysis, Piomelli et al. [41] gave the name *a priori* test to point out that no actual LES is carried out. *A priori* test using experimental data enables the study of high-Reynolds number flows. For example, Liu et al. [30, 31] observed the high correlation property of the scale similarity model (SSM) in isotropic turbulence using particle image velocimetry (PIV) data. In 1996, Menon et al. [35] compared various SGS models at tensor, vector and scalar level using DNS data. A one-equation model named the subgrid kinetic energy model (KEM) showed, consistently, a higher correlation for a range of Reynolds number when compared to other eddy-viscosity models, such as the Smagorinsky model (SM, Smagorinsky [47]), and the dynamic Smagorinsky model (DynSM, [19, 29]).

[†]Corresponding author. E-mail: haolu@wisc.edu;

[‡]E-mail: rutland@engr.wisc.edu;

[§]E-mail: lsmith@math.wisc.edu

SGS models have been used to simulate rotating turbulence [23, 26, 40]. However, there still exists a need for a better understanding of SGS models, because the above-mentioned *a priori* studies were not applied to rotating turbulence. At least two issues should be considered.

- Algebraic eddy-viscosity models (e.g. SM, DynSM and KEM) predict the global dissipation fairly accurately and have been widely used [40, 47]. Through these models, the small scales drain energy from the large scales. However, energy transfer from small to large scales is known to occur, especially in anisotropic turbulence. For rotating flows, although the rotation term (the Coriolis term) does not explicitly show up in the kinetic energy equation, rotation has an immediate effect on energy transfer and weakens the fundamental property of the energy cascade [3, 8, 33]. One might expect that eddy-viscosity models will have difficulty capturing this process [54].
- Most SGS models (e.g. eddy-viscosity models and SSM) are based on the assumption that the modeled small-scale turbulence is nearly homogeneous and isotropic, and do not account for Coriolis forces [55]. In rotating turbulence, coherent structures are changed by interactions between resonant velocity modes and between near-resonant modes [50–52]. In the present research, we find that the different micro-length scales occur in different directions and that this property can influence LES modeling. The performance of various SGS models is questioned because of these anisotropic properties, and alternative candidates have been proposed [24, 26, 46].

The present work is an *a priori* study of SGS models. DNS data at moderate Reynolds and Rossby numbers are used to validate models. We consider the flow of an initially very low energy level isotropic random noise which then undergoes either large-scale forcing or small-scale forcing. Such problems have been studied extensively in the past in both experiments and numerical simulations [28, 50].

The focus of this research is to study the performance of various SGS models and to develop models better suited to rotating turbulence. First, we discuss rotation effects and examine if the SGS models are consistent with the transformation properties of the SGS stress tensor in a non-inertial frame of reference undergoing rotation [46, 53, 54]. Kobayashi and Shimomura [26] and Horiuti [24] developed several consistent models of rotating turbulence and obtained encouraging results. These models are consistent with the material frame indifference (MFI) requirement for rotating flows. The consistent models are zero-equation models (e.g. algebraic closures), and not likely to satisfy the requirement that the trace of the SGS model equals twice the subgrid kinetic energy: $\tau_{ii}^{\text{model}} = 2k_{\text{sgs}}$. Hence, we present two new one-equation approaches to LES for rotating turbulence. These new models are consistent with the constraints of MFI, and also satisfy the trace requirement.

The primary tools we use for the *a priori* study are the regression and correlation coefficients. The correlation coefficient, ρ , was introduced by Clark et al. [14] in 1979 to study whether modeled and exact terms are related. If τ_{ij}^{model} and τ_{ij} are totally unrelated, then $\rho(\tau_{ij}, \tau_{ij}^{\text{model}}) = 0$. If there is a linear relation, then $\rho(\tau_{ij}, \tau_{ij}^{\text{model}}) = 1$. The correlation coefficient describes the strength of an association between two variables, and is completely symmetrical. The correlation between τ_{ij}^{model} and τ_{ij} is the same as the correlation between τ_{ij} and τ_{ij}^{model} .

In this study, we introduce the regression coefficient as another coefficient to examine the performance of models. The regression coefficient represents how much τ_{ij}^{model} changes with any given change of τ_{ij} and can be used to construct a regression line on a scatter plot of the two variables. For high-correlation models ($\rho > 0.6$ over a wide range of filter sizes), such as the SSM and the gradient model (GM), the regression coefficient is often more useful than the correlation coefficient. It gives a more complete description of the relationship between the two variables. A unit regression coefficient means that the modeled variable has the same magnitude as the variable obtained from the filtered DNS.

The paper is organized as follows. Section 2 provides a brief overview of LES and numerical issues. Section 3 discusses the anisotropy of rotating turbulence, the physical and the mathematical constraints for SGS models, and introduces two new one-equation models. Results of *a priori* tests of isotropic and rotating turbulence are presented in section 5. Preliminary *a posteriori* test results are included in section 6. Section 7 summarizes the findings. Appendixes include results from a different rotating case and a higher resolution real-viscosity rotating case to indicate that the findings are not unique to the cases presented.

2. SGS models and numerical methods

2.1 LES of rotating turbulence and SGS models

In LES, the Navier–Stokes equations of incompressible flow in a rotating frame are filtered using a spatial filter

$$\frac{\partial \bar{u}_i}{\partial x_i} = 0, \quad \frac{\partial \bar{u}_i}{\partial t} + \frac{\partial \bar{u}_i \bar{u}_j}{\partial x_j} = -\frac{\partial \bar{p}}{\partial x_i} - 2\epsilon_{ijk} \Omega_j \bar{u}_k + \nu \frac{\partial^2 \bar{u}_i}{\partial x_j \partial x_j} - \frac{\partial \tau_{ij}}{\partial x_j}, \quad (1)$$

where “ $\bar{\cdot}$ ” represents a convolution integral $\bar{f}(\vec{x}) = \int f(\vec{x}') G(\vec{x}, \vec{x}'; \Delta) d\vec{x}'$ with a filter function $G(\vec{x}, \vec{x}', \Delta)$, p is the effective pressure, ν is the kinematic viscosity, and Ω_i is the (constant) rotation rate. Without loss of generality, we chose $\vec{\Omega} = (0, 0, \Omega)$. Thus, the Coriolis term can be written as $-2\Omega \epsilon_{ijk} \bar{u}_k$. The SGS stress tensor is defined as $\tau_{ij} = \overline{u_i u_j} - \bar{u}_i \bar{u}_j$, where, on purpose, we have not subtracted the trace. Closure is obtained through modeling of the SGS stress.

The SGS stress tensor τ_{ij} can be decomposed into three parts, the modified Leonard term L_{ij}^M , the modified cross term C_{ij}^M and the modified SGS Reynolds stress term R_{ij}^M (Pope [44] and Geurts [20]),

$$\tau_{ij} = L_{ij}^M + C_{ij}^M + R_{ij}^M, \quad (2)$$

where $L_{ij}^M = \overline{\bar{u}_i \bar{u}_j} - \bar{u}_i \bar{u}_j$, $C_{ij}^M = \overline{\bar{u}_i u'_j} + \overline{u'_i \bar{u}_j} - \bar{u}_i \overline{u'_j} - \overline{u'_i} \bar{u}_j$, $R_{ij}^M = \overline{u'_i u'_j} - \overline{u'_i} \overline{u'_j}$. In addition, through use of the Gaussian filter, the SGS stress tensor can be expressed by a Taylor series (Pope [44], Leonard [27], Clark et al. [14] and Horiuti [21])

$$\tau_{ij} = \overline{u_i u_j} - \bar{u}_i \bar{u}_j = \frac{\Delta^2}{12} G_{ij} + O(\Delta^4), \quad \text{where } G_{ij} = \frac{\partial \bar{u}_i}{\partial x_k} \frac{\partial \bar{u}_j}{\partial x_k}. \quad (3)$$

As will be explained, some SGS models for τ_{ij} make explicit use of the decomposition (2), or the Taylor expansion (3).

A common class of SGS models describes the trace-free part of the SGS tensor by the form

$$\tau_{ij} - \frac{\tau_{kk}}{3} \delta_{ij} \approx -2\nu_t \bar{S}_{ij}, \quad (4)$$

where $\bar{S}_{ij} = \frac{1}{2}(\partial \bar{u}_i / \partial x_j + \partial \bar{u}_j / \partial x_i)$ and ν_t is the eddy viscosity. Several different models have been used for the eddy viscosity. On the basis of small scale statistical properties of isotropic turbulence, the first expression for the eddy viscosity ν_t was introduced in 1963 [47]. By the Smagorinsky Model (SM), the eddy viscosity is determined as

$$\nu_t = C_s^2 \Delta^2 |\bar{S}|, \quad (5)$$

where $|\bar{S}| = (2\bar{S}_{mn} \bar{S}_{mn})^{1/2}$, and C_s is a dimensionless coefficient. For complex flows, it may not be possible to find a universal coefficient that is appropriate for the entire domain at all times.

The subgrid kinetic energy model (KEM) is another widely used eddy-viscosity model [16, 25, 35], by which the full SGS stress is modeled as

$$\tau_{ij} \approx \frac{2}{3} k_{\text{sgs}} \delta_{ij} - 2\nu_k \bar{S}_{ij}, \quad (6)$$

where $k_{\text{sgs}} = \frac{1}{2} (\overline{u_k u_k} - \bar{u}_k \bar{u}_k) = \tau_{kk}/2$ is the SGS kinetic energy, and the SGS eddy viscosity is $\nu_k = C_k \sqrt{k_{\text{sgs}}} \Delta$. An approximation for k_{sgs} is obtained by solving the transport equation,

$$\frac{\partial k_{\text{sgs}}}{\partial t} + \bar{u}_j \frac{\partial k_{\text{sgs}}}{\partial x_j} = -\tau_{ij} \frac{\partial \bar{u}_i}{\partial x_j} - C_c \frac{k_{\text{sgs}}^{3/2}}{\Delta} + \frac{\partial}{\partial x_j} \left[\left(\frac{\nu_k}{\sigma_k} + \nu \right) \frac{\partial k_{\text{sgs}}}{\partial x_j} \right]. \quad (7)$$

Here, the three terms on the right-hand side of equation (7) represent, respectively, the production, dissipation, and diffusion of the SGS kinetic energy. The constants are typically chosen as $C_k = 0.05$, $C_c = 1.0$ and $\sigma_k = 1.0$ based on a previous study by Yoshizawa and Horiuti [58]. Through this one-equation approach, the KEM improves the accuracy of SGS stress modeling when compared to other eddy-viscosity models [35].

Eddy-viscosity models assume that the principal axes of the strain rate tensor are aligned with those of the SGS tensor. But, at the *a priori* test level, the SGS stress tensor correlates very poorly with the rate of strain tensor [14, 30, 35]. Furthermore, eddy-viscosity models are purely dissipative—energy only flows from resolved to subgrid scales. For numerical stability, this is a desirable characteristic. However, the actual SGS stress may also facilitate energy transfer from subgrid to resolved scales in a process referred to as ‘backscatter’ in isotropic turbulence. Furthermore, in anisotropic turbulence there can be a net transfer of energy from subgrid scales to resolved scales [50, 51].

To address some of the problems with eddy-viscosity models, the original scale similarity model was proposed in 1980 [1]. We study a modified version of the scale similarity model (SSM) which satisfies Galilean invariance [53, 54]

$$\tau_{ij} \approx C_L L_{ij}^M, \quad (8)$$

where C_L is a dimensionless coefficient—the so-called similarity coefficient.

By the definition of L_{ij}^M , implementation of the SSM requires a second filtering operation (test filtering) on the resolved field. At the *a priori* test level, the SSM successfully predicts the structure of the SGS stress tensor over a wide range of filter sizes. The SSM also allows for ‘backscatter.’

A different modeling approach uses the Taylor expansion (3) of τ_{ij} resulting in the gradient model (GM)

$$\tau_{ij} \approx \frac{\Delta^2}{12} G_{ij}. \quad (9)$$

The GM has several advantages: it is computationally efficient because it is a zero-equation model and does not require test filtering; it satisfies Galilean invariance and modeled stresses are consistent with the constraints of material frame indifference (see section 3.2); at the *a priori* test level, it successfully predicts the structure of the SGS stress tensor over a wide range of filter sizes; it allows for ‘backscatter’.

2.2 Pseudo-spectral method and forcing schemes

DNS validation cases were simulated using a pseudo-spectral code, which is similar to codes used in several previous studies [36, 37, 49–51, 57]. In these codes, the linear viscosity and Coriolis terms are included with an integrating factor, which is helpful to increase numerical

stability and to decrease numerical diffusion. We carried out the time advance in wave number space through the use of an explicit third-order Runge–Kutta scheme.

We consider flow under the influence of either large-scale or small-scale forcing. For large-scale forced isotropic turbulent runs, we compared the results using both Gaussian white-noise and Overholt–Pope’s [38] forcing scheme. The results are insensitive to the forcing scheme, but that the approach to statistically steady state was faster using the Overholt–Pope’s forcing. The case of isotropic turbulence has been performed using the Overholt–Pope’s scheme with parameters $\zeta = 0.25$, $T_f^* = 0.4$, $\alpha_c = 2\sqrt{2}/\tau$ and $\alpha = 0.7$.

In rotating and other anisotropic turbulent flows, Gaussian white-noise forcing allows for study of the nonlinear interactions with minimal bias from the forcing. Thus for our rotating turbulent runs, with an energy source at either large or small scales, we use white-noise forcing with Gaussian spectrum

$$F(k) = \epsilon_f \frac{\exp(-0.5(k - k_f)^2/\sigma^2)}{(2\pi)^{1/2}\sigma}, \quad (10)$$

where the standard deviation is $\sigma = 1$ and the energy input rate is $\epsilon_f = 1$ [48, 50, 51].

In order to study flow behavior over a wide inertial range, the dissipation at small scales was modeled according to the hyper-viscosity $(-1)^{p_u+1}v_u(\nabla^2)^{p_u}\vec{u}$ with $p_u = 8$ [6, 7]. In some cases, we add hypo-viscosity $(-1)^{p_i+1}v_i(\nabla^2)^{-p_i}\vec{u}$ with $p_i = 2$ to destroy box-size vortices. Drawing on both the work done by Chasnov [11] and dimensional analysis, we use

$$v_u = 2.5 \left(\frac{E(k_{\max}, t)}{k_{\max}} \right)^{1/2} k_{\max}^{2-2p_u}, \quad v_i = \left(\frac{E(k_{\min}, t)}{k_{\min}} \right)^{1/2} k_{\min}^{2+2p_i}, \quad (11)$$

where k_{\max} is the highest available wave number which is set according to the 2/3 de-aliasing rule [10], and where k_{\min} is the smallest wave number ($k_{\min} = 1$ on our isotropic grid).

2.3 Rossby numbers

Solid-body rotation does not rely on fluid velocity fields. In order to compare the inertial force with the Coriolis force, the Rossby number is studied, which characterizes the dimensionless ratio of the rotation time scale (the inverse of 2Ω) to a nonlinear time scale. Several different Rossby numbers can be defined, depending on how one chooses to estimate the nonlinear time scale. With a nonlinear time scale based on the parameters of the forcing (10), one Rossby number is defined as

$$\text{Ro}^G = \frac{(\epsilon_f k_f^2)^{1/3}}{2\Omega}. \quad (12)$$

Additionally, the macro-scale Rossby number Ro^L , and micro-scale Rossby number Ro^{ω_3} are defined by

$$\text{Ro}^L = u'/(2\Omega L), \quad \text{Ro}^{\omega_3} = \omega'_3/(2\Omega). \quad (13)$$

In these expressions u' is the root-mean-square (RMS) velocity fluctuation, ω'_3 is the RMS vorticity in the z -direction, $L = u'K/\varepsilon$ denotes a typical length scale, where K is the total kinetic energy, and ε is the dissipation rate of the total kinetic energy K . When the Rossby number is large (either because Ω is small, or because L is small, i.e. for small-scale motions such as flow in a bathtub, or for large speeds), the effects of rotation can be neglected. A small Rossby number indicates that the effects of rotation are comparably large.

We are considering the Rossby number as a criteria for concerning rotational effects on modeling of SGS stress. The Rossby number under ordinary conditions (walking speed

$u' = 5$ [MPH], $L = 1$ [m], planetary rotation) is about 15 000. Thus, Lumley [32] has stated that ‘the rotational effects on Reynolds stress can be disregarded and the principle of MFI (see section 3.2) is quite justified under ordinary conditions’. Lots of physical phenomena, however, do not have a large Rossby number, for instance; the Rossby number of a typical hurricane is ~ 1 , and the Rossby number of a typical gas turbine engine flow is ~ 0.3 . In this research, rotating flows are performed at small micro-scale Rossby numbers ~ 0.1 , which is an approximate Rossby number for flows in the gulf stream, and for synoptic-scale flows at mid-latitudes [39, 49]. For rotating turbulence at small micro-scale Rossby numbers, hence, we are not applying the principle of MFI to SGS stress at subgrid scales ([24], and also see section 3.2).

There are several challenges for LES of rapidly rotating flow with Rossby numbers less than unity. Accurate computations will reproduce at least three important features (some more prominent in forced flow as compared to decaying turbulence): (i) significant net transfer of energy from small to large scales, (ii) the generation of large-scale vortical columns, with dominance of cyclones over anti-cyclones, and (iii) a tendency toward two-dimensional and two-component flow, with much lower levels of energy in the velocity component parallel to the rotation axis. Furthermore, studies have suggested that numerical simulations are restricted by resolution constraints to moderately small Rossby numbers less than unity [8, 49]. With guidance from previous studies, we have performed simulations over a range of Rossby numbers $0.1 < \text{Ro}^{\omega^3} < 0.4$ [4], $\text{Ro}^L < 1$ [8] and $\text{Ro}^G \approx 0.1$ [49].

3. Building new models

Most classical models are based on the assumption of small-scale isotropy. For instance, the SSM uses a single coefficient C_L to set the magnitudes of all six modeled stress components (τ_{ij}). For rotating turbulence, however, it is not clear if isotropy is achieved even at the smallest scales of motion.

3.1 Anisotropy of rotating turbulence

In previous studies, integral length scales were used to investigate nonlinear interactions modified by rotation [8, 9]. In LES modeling, however, we focus on Taylor micro-scales because it is expected that these are impacted more by the SGS model performance. Introduced by Taylor [56] in 1935, micro-scales are expressed as

$$\lambda_{ij}^k = \sqrt{2\langle u_i \rangle \langle u_j \rangle / (\langle \partial u_i / \partial x_k \rangle \langle \partial u_j / \partial x_k \rangle)}, \quad (14)$$

where $\langle \cdot \rangle$ represents the arithmetic mean. Longitudinal micro-scales are defined by $\lambda_{f,i} = \lambda_{ii}^i$ (no summation), and transverse micro-scales are defined by $\lambda_{g,ik} = \lambda_{ii}^k$ (no summation).

Isotropic turbulence has identical longitudinal and transverse micro-scales (see figure 4). However, as shown in figure 1, the longitudinal micro-scale in the z -direction of a typical rotating turbulence (specified in section 4) is smaller than the scales in other directions

$$\lambda_{f,3} < \lambda_{f,1}; \quad \lambda_{f,3} < \lambda_{f,2}. \quad (15)$$

These relations are universally true for all rotating turbulent cases in this research, and they are used to explain the influence of anisotropy on LES modeling in section 5.3.2.

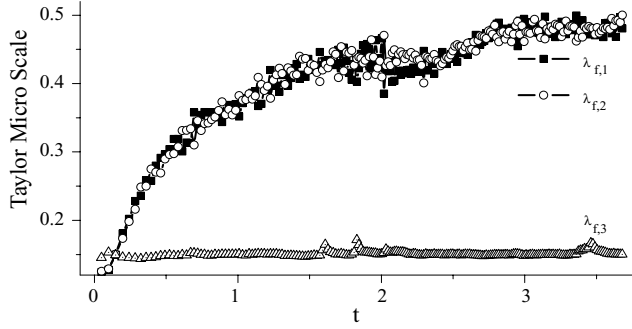


Figure 1. Evolutions of Taylor micro-scale, in small-scale forced rotating turbulent case B5. Time is normalized by final eddy turn-over time.

3.2 The invariance of SGS models

With a view toward developing models that are more suitable for the LES of rotating turbulence, it is helpful to consider the invariance properties of the full equations and of models.

First, Galilean invariance of LES modeling has been studied for over 20 years [53]. The Navier–Stokes equations as well as their filtered form (1) are invariant under the Galilean group of transformations, $\mathbf{x}^* = \mathbf{x} + \mathbf{V}t + \mathbf{B}$. The SGS stress tensor is also invariant, $\tau_{ij} = \tau_{ij}^*$, under the Galilean transformation. As a cautionary remark, SGS models are required to exhibit the same (invariant) feature as the SGS stress tensor. Fortunately, except the original scale similarity model ($\tau_{ij} \approx \overline{u_i u_j} - \overline{u_i} \overline{u_j}$) by Bardina [1], all other recent models satisfy Galilean invariance.

Second, the consistency with material frame indifference (MFI) has been considered as one constraint of SGS models under the Euclidean group of transformations, $\mathbf{x}^* = \mathbf{Q}(t) \cdot \mathbf{x}$ [24, 26, 46, 54]. Here, let us review the previous works in brief. We denote a proper orthogonal rotation matrix ($\mathbf{Q} \cdot \mathbf{Q}^T = \mathbf{I}$) as Q_{ij} , and x_i^* (u_i^*) is the position (velocity) vector in a rotating frame. The principle of MFI ($Q_{ia} t_{ab} Q_{bj}^T = t_{ij}^*$, where t_{ij} are components of an arbitrary tensor) has been applied as a principle for constitutive relations in Navier–Stokes equations [45]. However, the SGS stress tensor τ_{ij} in an inertial frame is connected to the SGS stress tensor $\tau_{ij}^* = \overline{u_i^* u_j^*} - \overline{u_i^*} \overline{u_j^*}$ in a rotating frame according to a frame different expression

$$Q_{ia} \tau_{ab} Q_{bj}^T = \tau_{ij}^* + Z_{ij}^*, \tag{16}$$

where Z_{ij}^* is given by

$$\begin{aligned} Z_{ij}^* = & \epsilon_{iab} \Omega_a^* (\overline{x_b^* u_j^*} - \overline{x_b^*} \overline{u_j^*}) + \epsilon_{jab} \Omega_a^* (\overline{x_b^* u_i^*} - \overline{x_b^*} \overline{u_i^*}) \\ & + \epsilon_{iab} \epsilon_{jcd} \Omega_a^* \Omega_c^* (\overline{x_b^* x_d^*} - \overline{x_b^*} \overline{x_d^*}), \end{aligned} \tag{17}$$

and where Ω_i^* is the angular velocity of the rotating frame. For the Gaussian filter, the quantity Z_{ij}^* is analytically expanded to be

$$Z_{ij}^* = \frac{\Delta^2}{12} \left(\epsilon_{iab} \Omega_a^* \frac{\partial \overline{u_j^*}}{\partial x_b^*} + \epsilon_{jab} \Omega_a^* \frac{\partial \overline{u_i^*}}{\partial x_b^*} + \Omega_a^* \Omega_a^* \delta_{ij} - \Omega_i^* \Omega_j^* \right) + O(\Delta^4). \tag{18}$$

This Taylor expansion shows that the rotational effects on τ_{ij} and LES models decay as (Δ^2) . Furthermore, it can be shown that the tensor Z_{ij}^* is divergence free with $\partial Z_{ia}^* / \partial x_a^* = 0$, leading

to frame indifference of the vector $\partial\tau_{ij}^*/\partial x_j^*$:

$$Q_{ia} \frac{\partial\tau_{ab}}{\partial x_b} = \frac{\partial\tau_{ia}^*}{\partial x_a^*}. \quad (19)$$

Since $\partial\tau_{ij}/\partial x_j$ appears in the LES momentum equation (1), and not the tensor τ_{ij} itself, one may argue that SGS models need only to satisfy the MFI-consistency on the vector level (19), rather than on both the vector (19) and the tensor levels (16). However, the stress tensor τ_{ij} itself is important for the SGS kinetic energy equation, and thus we adopt the point of view that as a rigorous principle, the a modeled stress tensor should satisfy, $Q_{ia}\tau_{ab}^{\text{model}}Q_{bj}^T = \tau_{ij}^{*,\text{model}} + Z_{ij}^* + (Z_{ij}^{*,\text{model}} - Z_{ij}^*)$ with $Z_{ij}^{*,\text{model}} - Z_{ij}^* = 0$, just as the exact stress tensor does in equation (16) [23, 24, 26, 46]. It is interesting to note that the ratio of τ_{ij} (and τ_{ij}^*) to Z_{ij}^* can also be characterized by the Rossby number. For rotating turbulence at small micro-scale Rossby numbers, as mentioned in section 2.3, we consider rotational effects for small-scale turbulence. Otherwise, SGS modeling error caused by rotational frame transfers, $Z_{ij}^{*,\text{model}} - Z_{ij}^*$, will be added into a fluid dynamic system for different rotational frames (inertial frame: $\Omega = 0$). Speziale [54] has stated that without concerning the effects of rotation, eddy-viscosity models have difficulties to predict energy transfers between resolved and subgrid scales when $\Omega \rightarrow \infty$. If the rotation rate of the framing is increased, the GM (9), one of the MFI-consistent SGS models has the correct damped-dissipation behavior for rotating turbulence [54]. Requiring (16), some classical SGS models, such as the SM and the SSM, are inconsistent with MFI. It has been stated that the GM and the sum of L_{ij}^M and C_{ij}^M are consistent with this constraint ([46, 52], sometimes referred to as ‘form invariant’).

3.3 Dynamic structure model

A dynamic one-equation non-viscosity model named the dynamic structure model (DSM) was recently introduced by Pomraning and Rutland [42, 43]. The DSM uses a tensor form of SGS stresses: $\tau_{ij} = C_{ij}k_{\text{sgs}}$. Note that C_{ij} must satisfy $C_{ii} = 2$. Assuming the same form at the test filtering level, $T_{ij} = \widetilde{u_i u_j} - \widetilde{u_i} \widetilde{u_j} = C_{ij}K$, and substituting into the Germano [18] identity, one finds

$$T_{ij} - \widetilde{\tau}_{ij} = \widetilde{u_i u_j} - \widetilde{u_i} \widetilde{u_j} = C_{ij}K - C_{ij}\widetilde{k}_{\text{sgs}} \approx C_{ij}(K - \widetilde{k}_{\text{sgs}}). \quad (20)$$

For this model, the structure of the SGS stress tensor is extracted from the Leonard term and the SGS kinetic energy is used to predict the magnitude. For equal test and grid filter sizes, the DSM reduces to an algebraic model for the SGS stress tensor of the form

$$\tau_{ij} \approx \left(\frac{L_{ij}^M}{L_{mm}^M} \right) 2k_{\text{sgs}}. \quad (21)$$

3.4 Consistent dynamic structure models

Even though the original DSM has been shown to have excellent agreement with the exact SGS stresses for isotropic turbulence [13, 42], it does not satisfy the consistency of frame transfer with the exact SGS stress. Thus, for rotating turbulence, we developed two models in the DSM family that are consistent with MFI.

Recall that the stresses corresponding to the gradient model (9) are consistent with the constraints of MFI [26]. Thus, we introduce the gradient-type consistent dynamic structure

model (GCDSM) for rotating flows

$$\tau_{ij} \approx \left(\frac{G_{ij}}{G_{mm}} \right) 2k_{\text{sgs}} \quad \text{where } G_{ij} = \frac{\partial \bar{u}_i}{\partial x_k} \frac{\partial \bar{u}_j}{\partial x_k}. \quad (22)$$

A second model can be formed using the fact that $L_{ij}^M + C_{ij}^M$ is consistent with the constraints of MFI [46, 54]. We introduce the similarity-type consistent dynamic structure model (SCDSM) with the form

$$\tau_{ij} \approx \left(\frac{\Upsilon_{ij}}{\Upsilon_{mm}} \right) 2k_{\text{sgs}}, \quad (23)$$

where the sum of the Leonard term and the cross term is modeled as Υ_{ij} ,

$$\Upsilon_{ij} = C_L L_{ij}^M + C_C [(\overline{\bar{u}_i \bar{u}_j} - \bar{\bar{u}_i} \bar{\bar{u}_j}) + (\overline{\bar{u}_i \bar{u}_j} - \bar{\bar{u}_i} \bar{\bar{u}_j}) - 2(\overline{\bar{u}_i \bar{u}_j} - \bar{\bar{u}_i} \bar{\bar{u}_j})]. \quad (24)$$

When the cross term C_{ij}^M is approximated in the form of the generalized scale similarity model [22], C_C and C_L are both $O(1)$ dimensionless coefficients. In this research, C_C is set to 1.5, and C_L is set to 1.

4. Case descriptions

Once fully developed turbulent flows were achieved, *a priori* tests of various SGS models could be performed. As mentioned above, both isotropic turbulence and rotating turbulence cases were used, and ultimately the goal is to demonstrate the improved performance of the new models GCDSM (22) and SCDSM (23). Here we introduce the main cases: isotropic turbulence forced at large scales (case A), rotating turbulence forced a small scales (B series), rotating turbulence forced at large scales (C series). In all cases, the domain is a periodic cube of volume $(2\pi)^3 [m^3]$ and flows are resolved using 128^3 Fourier modes. All flows were initialized with low energy isotropic noise, and the force was turned on at time zero.

Case A is an isotropic turbulence forced at large scales ($1.9 < k_f < 4.5$) using an Overholt-Pope's forcing scheme. A kinematic viscosity of $0.0013 [m^2/s]$ leads to a statistical steady state with a Taylor micro-scale Reynolds number $Re_\lambda = 100$. The spectrum of the final state is shown in figure 2. The wave number is normalized by the Kolmogorov length scale, $\eta = (v^3/\varepsilon)^{1/4} = 0.01 [m]$, and for convenience, a $-5/3$ power law is shown as a dotted line. Figure 3 shows the evolutions of the kinetic energy, and the micro-scale Reynolds number indicates that

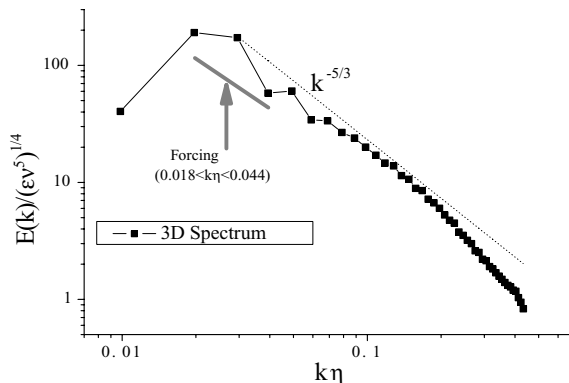


Figure 2. Energy spectrum of the final statistical steady state of isotropic turbulent case A.

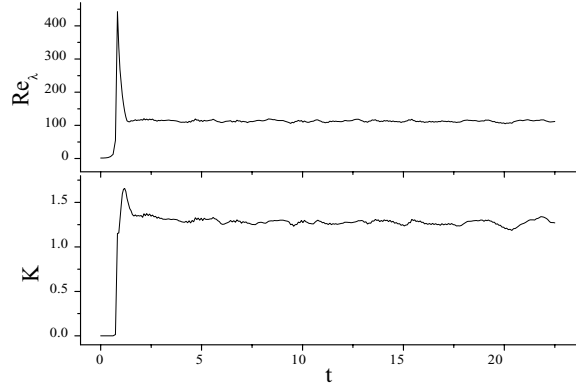


Figure 3. Evolutions of kinetic energy and micro Reynolds number of isotropic turbulent case A. Time is normalized by final eddy turn-over time.

a statistical steady state has been reached. As discussed above, figure 4 indicates the isotropy of the flow characterized by the micro-length-scale feature $\lambda_{f,i}/\lambda_{g,jk} = \sqrt{2}$, ($j \neq k$) [44].

For rotating turbulence, we performed a series of simulations B and C, with case names, parameters and final Rossby numbers given in table 1. As mentioned, a Gaussian white-noise force is used for both series B and C, with the peak wave number of the force as the main difference between the two sets of runs: series B has small-scale forcing with the peak wave number $k_f = 11$ or $k_f = 21$, and series C has large-scale forcing with the peak wave number $k_f = 2.5$. Runs B1–B4 are time developing without large-scale damping, and are terminated before energy accumulates in box-size vortices corresponding to population of modes with $k = 1$. Note that energy is growing in those runs and only scales smaller than the forcing scale are in a statistically steady state. Case B5 and C series run have hypo-viscosity to remove box-size vortices, and would eventually reach a statistically steady state at all scales. For all B

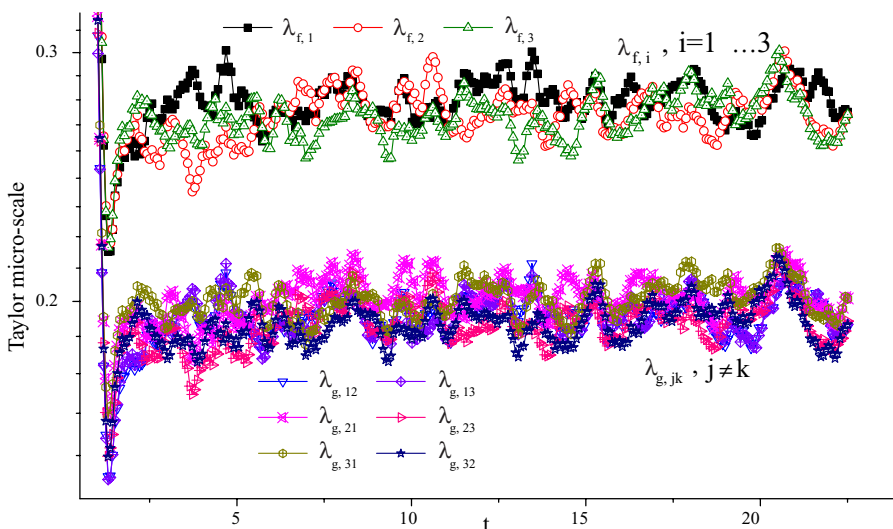


Figure 4. Evolutions of Taylor micro-scale, in isotropic turbulent case A. Time is normalized by final eddy turn-over time. Numerically, $\lambda_{f,i}/\lambda_{g,jk} = \sqrt{2}$, ($j \neq k$) is illustrated.

Table 1. Description of forced rotating runs.

Case	k_f	Ω (rad s ⁻¹)	Viscosity	Ro^G	Ro^{ω_3}
B1	11	10	Hyper only	0.25	0.38
B2	11	50	Hyper only	0.049	0.094
B3	21	10	Hyper only	0.38	0.38
B4	21	50	Hyper only	0.076	0.082
B5	21	50	Hyper + hypo	0.076	0.086
C1	2.5	2	Hyper + hypo	0.46	0.50
C2	2.5	4	Hyper + hypo	0.23	0.31
C3	2.5	6	Hyper + hypo	0.15	0.35
C4	2.5	8	Hyper + hypo	0.12	0.24

and C series runs, the rotation rate was carefully selected to achieve moderately small values of Rossby numbers Ro^G and Ro^{ω_3} (see section 2.3).

Figures 6 and 7 show spectra from case B5 and case C3. Both figures show that energy in the large scales is predominantly in two-dimensional modes, while energy at small scales is increasingly three-dimensional. Figure 6 shows that, with forcing at small scales, the scaling of the large-scale spectrum of rotating turbulence is in steeper energy spectrum $E(k) \approx E(k_h, k_z = 0) \propto k_h^{-3}$, $k_h = \sqrt{k_x^2 + k_y^2}$ [49]. The physical space pictures corresponding to the spectra of figures 6 and 7 are shown in figure 8, with quasi two-dimensional cyclonic vortical columns in both cases. Similar coherent structures and *a priori* test results are obtained from all cases. In the main text, we present *a priori* test results for case B5, and results for case C3 are presented in the appendix.

5. *A priori* test

5.1 Correlation and regression

A common method of evaluating SGS models is through *a priori* tests in which models are compared to filtered DNS results. This serves as a standard testing technique for SGS models

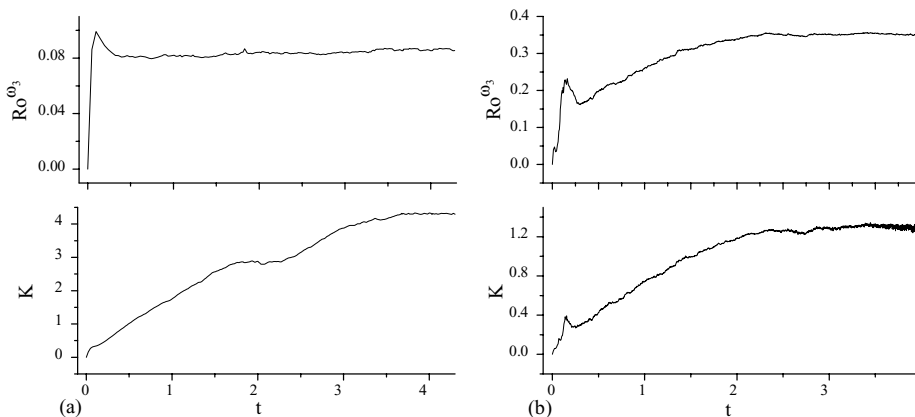


Figure 5. Evolutions of kinetic energy and Ro^{ω_3} : (a) small-scale forced rotating case B5; (b) large-scale forced rotating case C3. Time is normalized by final eddy turn-over time.

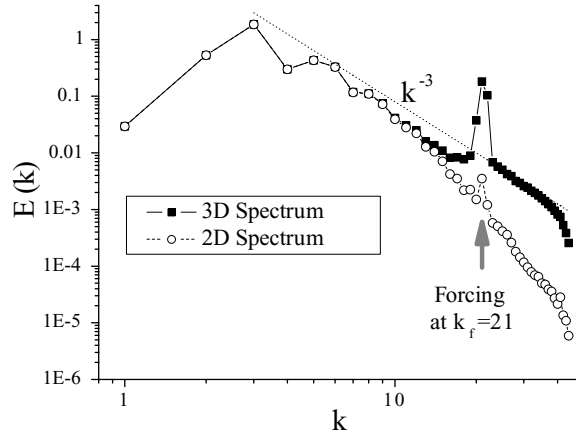


Figure 6. Energy spectrum of the final state of rotating turbulent case B5.

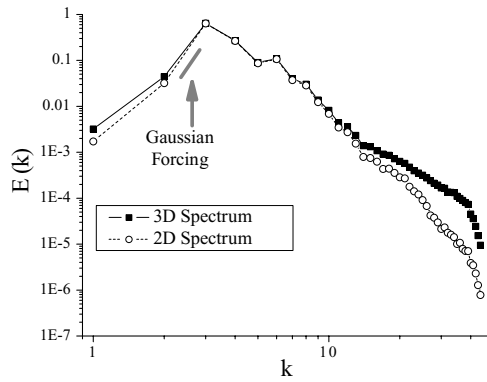
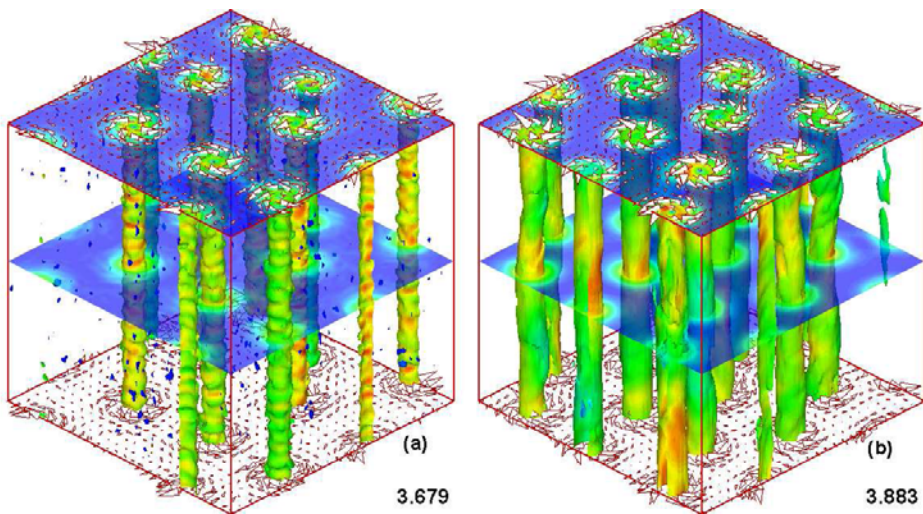


Figure 7. Energy spectrum of the final state of rotating turbulent case C3.

Figure 8. Cyclonic two-dimensional coherent structures appearing in rotating turbulence as indicated by iso-surfaces of vorticity, contours of kinetic energy and velocity vectors: (a) final state (at $time = 3.68$) of small-scale forced rotating case B5. (b) final state (at $time = 3.88$) of large-scale forced rotating case C3.

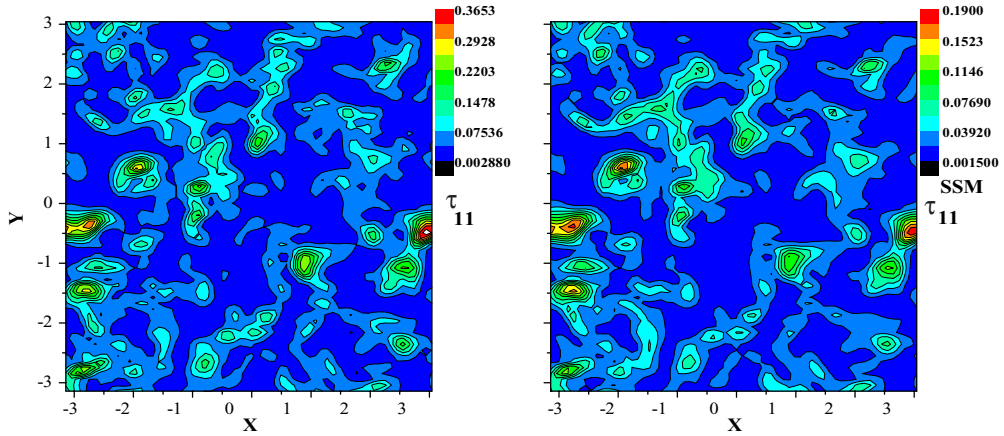


Figure 9. Comparison of contour plots of SGS stress τ_{11} (left) and scale similarity modeled stress τ_{11}^{SSM} (right) at $z = 0$ layer, in isotropic turbulent case A (Resolution: 128^3). Parameters for the SSM: $k_c = 32$ and $C_L = 1$. τ_{11} and τ_{11}^{SSM} have similar structures but different contour levels. The contour level ratio is given by regression coefficient: $\beta(\tau_{11}, \tau_{11}^{SSM}) = 0.52$.

that is used as an initial evaluation and comparison of models. Later, in future work, tests of the most promising models will be made using LES codes in *a posteriori* tests.

A qualitative *a priori* evaluation can be made by comparing representative contour plots such as the ones shown in figure 9. Here τ_{11} from the SSM and a filtered DNS simulation of isotropic flow are compared. The model can duplicate much of the general structure of τ_{11} , but the magnitudes of the contour levels are significantly different. This evaluation helps to reveal which models duplicate more details of SGS stresses and which models are designed to capture the average behavior but may miss details.

More quantitative *a priori* evaluations can be made using probability density functions (PDF) of relative errors such as $E = (\tau_{ij}^{model} - \tau_{ij})/\tau_{ij}$ shown in figure 10 [12], and by scatter plots of modeled terms versus filtered DNS terms as shown in figure 11. In many situations, the main character of the scatter plots can be described by a linear regression. The linear regression equation, $b = \beta \cdot a + \alpha$, represents the relationship between variables a and b . The slope of the linear correlation line, β , and the scatter around this correlation line, ρ , provide

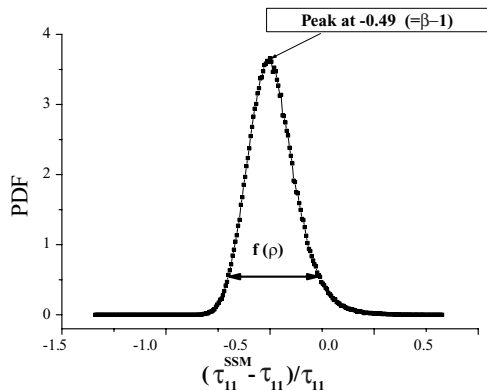


Figure 10. PDF of the relative errors of τ_{11} . Same settings as figure 9. Peak position can be calculated via $\beta - 1$.

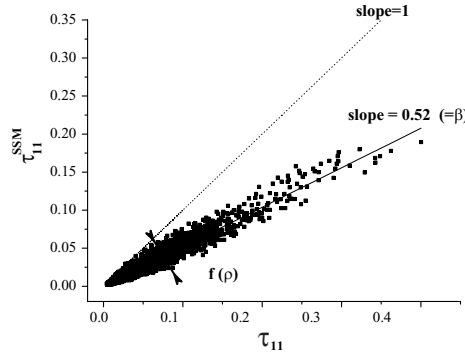


Figure 11. Scatter plot of τ_{11} . Same settings as figure 9. Slope of the scatter line is predicted by regression coefficient β directly.

convenient measures of SGS models in *a priori* tests. Note that β is related to the ratio of the contour levels in figure 9, to the mean of the error PDF in figure 10 and to the slope of the linear curve fit in figure 11. Also, ρ is related to the variance of the PDF in figure 10 and to the scatter around the linear line in figure 11. Generally, $\alpha = 0$ in LES modeling.

Conventionally, β is called the regression coefficient and ρ is called the correlation coefficient. The regression coefficient is evaluated by a least squares fit leading to

$$\beta(a, b) = \frac{\langle ab \rangle - \langle a \rangle \langle b \rangle}{\langle a^2 \rangle - \langle a \rangle^2}, \quad (25)$$

with the optimal value $\beta = 1$. The correlation coefficient is evaluated by

$$\rho(a, b) = \frac{\langle ab \rangle - \langle a \rangle \langle b \rangle}{\sqrt{(\langle a^2 \rangle - \langle a \rangle^2)(\langle b^2 \rangle - \langle b \rangle^2)}}. \quad (26)$$

The range of ρ is -1 to 1 with negative values of ρ rarely occurring in LES *a priori* testing and values close to one indicating a strong correlation.

The two coefficients β and ρ are global factors rather than local factors. A decrease from the value $\rho = 1$ in the correlation indicates a loss of ability of capturing the correct resolved flow structure, and a departure from the value $\beta = 1$ in the regression indicates a loss of ability of capturing the correct magnitude level of resolved flow quantities. Menon et al. [35] showed that even when there was similarity between the resolved structures, the peak values predicted by the SSM could be quite different from the exact values (about 25% lower for their cases). The regression coefficient can be used to describe this difference quantitatively.

The regression and correlation coefficients are the primary tools used in the current *a priori* tests. Several different aspects of the SGS models are tested. Tests of individual tensor components as the terms a and b in equations (26) and (25) are indicated by dual subscripts: $\rho_{ij} = \rho(\tau_{ij}, \tau_{ij}^{\text{model}})$ and $\beta_{ij} = \beta(\tau_{ij}, \tau_{ij}^{\text{model}})$. Tests of the components of the divergence of τ_{ij} , which appears in the momentum equation, are indicated by single subscripts: $\rho_i = \rho(\frac{\partial \tau_{ij}}{\partial x_j}, \frac{\partial \tau_{ij}^{\text{model}}}{\partial x_j})$ and $\beta_i = \beta(\frac{\partial \tau_{ij}}{\partial x_j}, \frac{\partial \tau_{ij}^{\text{model}}}{\partial x_j})$. Tests of the kinetic energy production term, $P = -\tau_{ij} \frac{\partial \bar{u}_i}{\partial x_j}$, are indicated by no subscripts: $\rho(P) = \rho(-\tau_{ij} \frac{\partial \bar{u}_i}{\partial x_j}, -\tau_{ij}^{\text{model}} \frac{\partial \bar{u}_i}{\partial x_j})$ and $\beta(P) = \beta(-\tau_{ij} \frac{\partial \bar{u}_i}{\partial x_j}, -\tau_{ij}^{\text{model}} \frac{\partial \bar{u}_i}{\partial x_j})$.

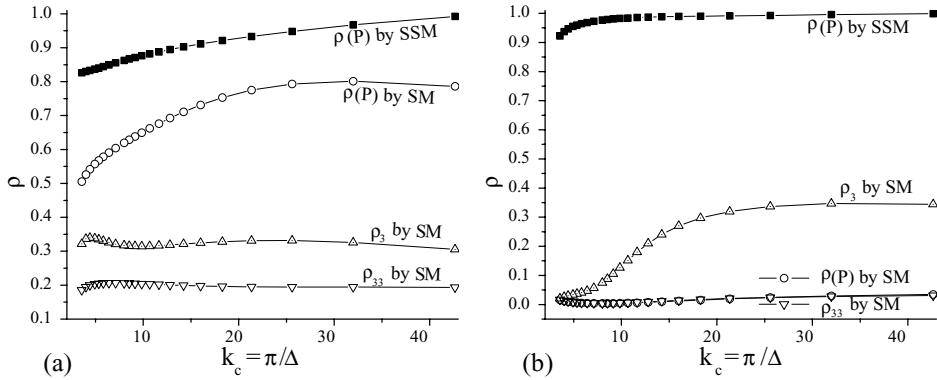


Figure 12. Correlation coefficient for SM: (a) isotropic case A; (b) rotating case B5.

5.2 Eddy-viscosity models

Eddy-viscosity models are low-correlation models. It has been well established that the strain rate tensor has a low correlation level ($\rho < 0.4$) with stress components [1, 14, 30, 35]. Similar results are obtained in our DNS cases and summarized below.

Figures 12 and 13 show correlation coefficients for SGS models in isotropic turbulence and rotating turbulence as a function of cut-off wave number, since there is no clear definition of the Kolmogorov scale for rotating flow. Results for the SSM are provided as a reference for comparison because it is known to be a relatively high-correlation model. All components of the SGS stress tensor and its divergence were examined but only representative components are presented.

For isotropic turbulence, the SM gives a low-correlation level (~ 0.2) for stress components (τ_{ij}), a slightly better correlation (~ 0.35) for the vector components of the divergence ($\partial\tau_{ij}/\partial x_j$), and a better correlation ($0.5 \sim 0.8$) for the production term. These results are consistent with the findings of Clark et al. [14], Liu et al. [30], Menon et al. [35] and others. For rotating turbulence, the SM gives very low-correlation coefficients ($0 \sim 0.03$) for stress components, higher correlations ($0.02 \sim 0.2$) for vector components of the divergence, and very low correlations ($0 \sim 0.03$) for the production term.

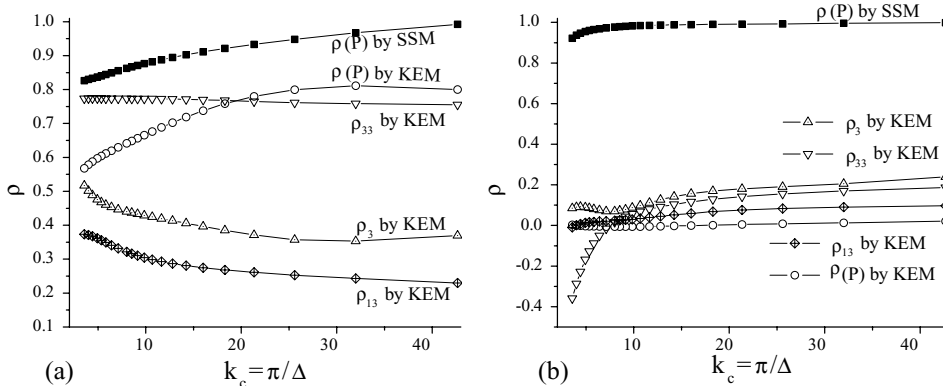


Figure 13. Correlation coefficient for KEM: (a) isotropic case A; (b) rotating case B5.

For isotropic turbulence, the KEM gives very good correlation coefficients (~ 0.8) for stress components (τ_{ij} , $i=j$), but a low-correlation level (~ 0.3) on cross terms (τ_{ij} , $i \neq j$). According to the definition of the KEM, these outcomes are reasonable because the magnitude of the diagonal terms is dominated by the SGS kinetic energy, while the cross terms are determined by the strain rate tensor. The correlation level of the components of the divergence is between 0.3 and 0.5, and the correlation level of the energy production term is between 0.5 and 0.8. These results are consistent with the previous findings of Menon et al. [35]. For rotating turbulence, the KEM gives a low-correlation coefficient ($\rho < 0.2$) for any stress component involving the rotation direction (τ_{3j} , $j=1,2,3$), for all components of the divergence, and for the energy production term. Significantly, it gives a negative ρ_{33} for very large filter sizes.

5.3 MFI-consistent models

Models that are MFI-consistent with the exact SGS stress are expected to do much better in rotating systems. These models have high correlation and regression coefficients and improved ability to capture the anisotropy of rotating turbulent flows.

5.3.1 Correlation of SGS models. Models based on the scale-similarity procedure or a Taylor expansion usually give high correlation coefficients in *a priori* tests. As mentioned in section 3.2, two new models have been developed based on these two procedures, the GCDSM and the SCDSM. As a consequence, they are able to capture the resolved flow structure much better than eddy-viscosity models.

Focusing on the SCDSM results, figure 14 shows the correlation coefficient ρ_i in the rotating turbulence case B5. Even though the correlation of the divergence component in the z -direction decreases more rapidly than the other components, all three correlations for the vector components are greater than 0.6 over a wide range of filter sizes. Similar results were obtained for tensor correlation coefficients, only ρ_{33} could be below 0.6 when $k_c < 10$ in some rotating turbulent cases.

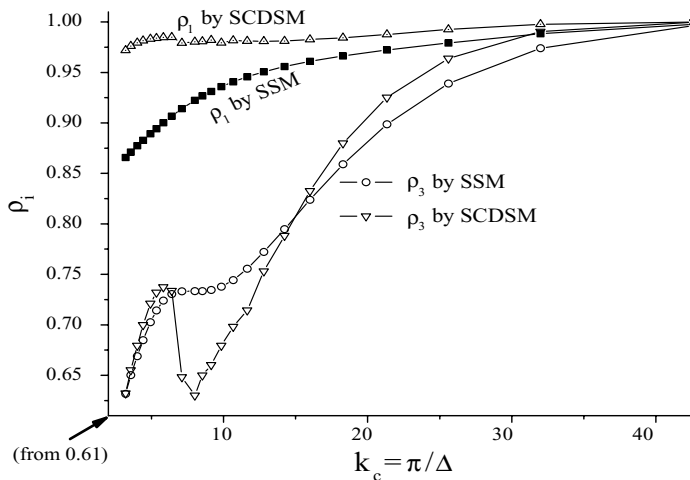


Figure 14. Correlation coefficient for rotating case B5.

5.3.2 Influence of anisotropy. Section 3.2 showed that SSM is inconsistent with MFI at the stress tensor level. Here, we use *a priori* test results to uncover its failure to capture anisotropy. We chose the SSM as an example because it is a widely used zero-equation SGS stress model. SCDSM is used as an example to show that MFI-consistent models are better able to capture anisotropy.

According to the definition of the SSM (8), all six modeled stress components use the same similarity coefficient, C_L . This coefficient has no influence on correlation but does change regression coefficients. The coefficient $C_L = 1$ has been used, so the regressions are close to 1 for very small filter sizes.

Figure 15 shows the correlation and regression coefficients of stress components in an isotropic case A and in a rotating turbulent case B5. Regardless of the flow type, the correlation and the regression coefficients decrease when the filter size increases (k_c decreases). These results show that the SSM becomes quite poor as the grid is coarsened.

As shown in figures 15(a) and (b), for isotropic turbulence, because of isotropy, the six correlation coefficients of stress components decrease similarly, and the six regression coefficients of stress components decrease similarly.

For rotating turbulence, the SSM correlation and regression coefficients that correspond to the rotating direction components decrease much more rapidly with filter size than the other coefficients, as shown in figures 15(c) and (d). This difference between the isotropic turbulence and the anisotropic turbulence lies in the length scales. Section 3.1 has shown that rotating turbulence does not have an identical scale in all directions. Generally, $\lambda_{f,3}$ is smaller than $\lambda_{f,1}$ and $\lambda_{f,2}$. When isotropic filters are used, the normalized length scale Δ/λ_f in the z -direction

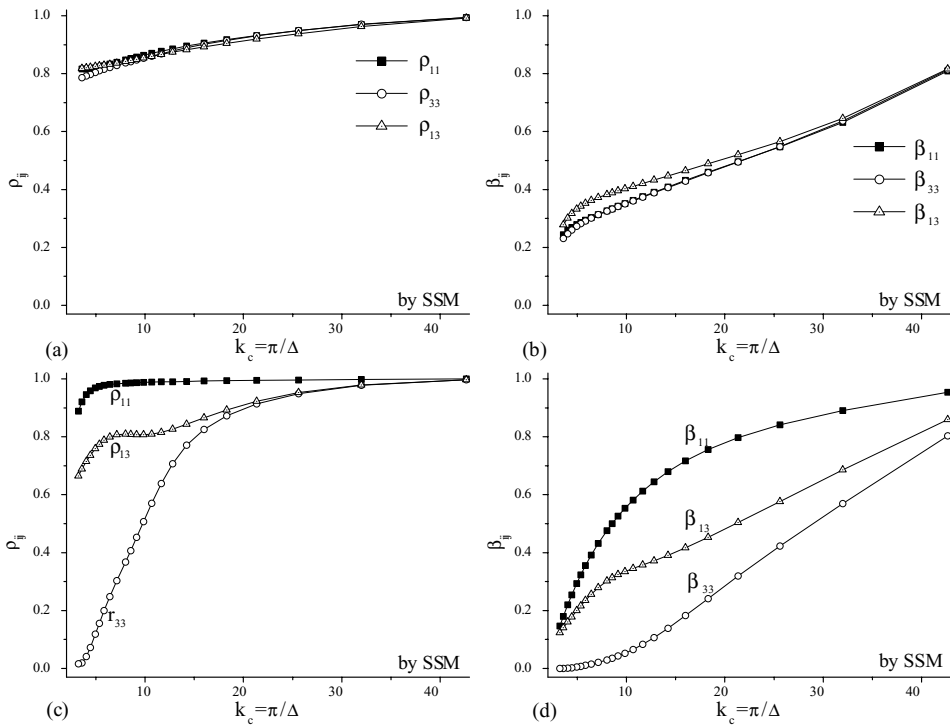


Figure 15. Correlation and regression coefficients: (a) $\rho(\tau_{ij}, \tau_{ij}^{SSM})$ and (b) $\beta(\tau_{ij}, \tau_{ij}^{SSM})$ in isotropic case A; (c) $\rho(\tau_{ij}, \tau_{ij}^{SSM})$ and (d) $\beta(\tau_{ij}, \tau_{ij}^{SSM})$ in rotating case B5.

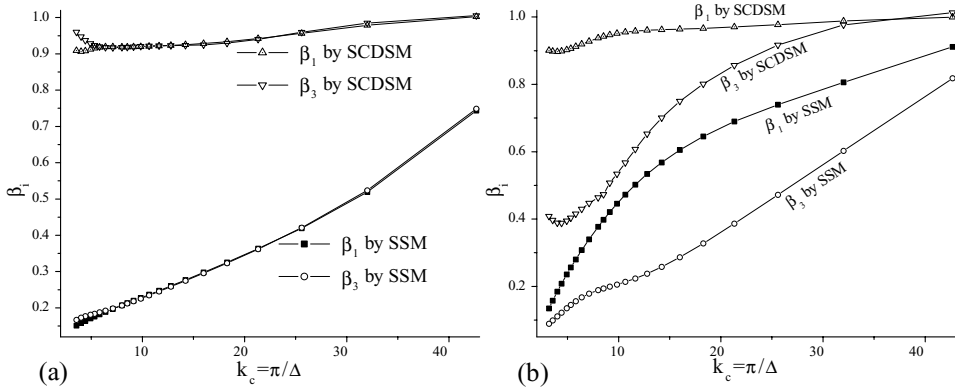


Figure 16. Regression coefficient: (a) isotropic case A; (b) rotating case B5.

is larger, and the turbulence details in the z -direction are more highly filtered. In a sense, a relatively coarser grid has been employed in the z -direction. As a consequence, the correlation and the regression coefficients associated with the z -direction components are smaller than for the other directions.

In contrast, the MFI-consistent SCDSM shows much better results than the SSM. Figures 16 shows the regression coefficients of vector components in case A and case B5 for the two models. For isotropic turbulence, the SCDSM gives nearly perfect regressions in all directions for all filter sizes, but SSM shows very poor regression coefficients. For rotating turbulence, anisotropy effects make the regressions in the z -direction decrease more rapidly. However, the SCDSM regression coefficients remain greater than 0.8 in all directions for smaller filter sizes ($k_c \geq 20$). In contrast, the SSM only gives $\beta_3 \approx 0.35$ when $k_c = 20$.

5.3.3 Regression of SGS models. For isotropic turbulence, figures 15(b) and 16(a) illustrate that the regression coefficient of the SSM decreases rapidly to values less than 0.35 when k_c decreases to 20. To improve the regression coefficient of models, at least two methods have been introduced in previous literatures. One method uses SGS kinetic energy to determine the similarity coefficient in the zero-equation scale similarity models [15]. This approach, however, has to use energy spectra in Fourier space, which may be not applicable to most engineering applications. In the method adopted herein, called the dynamic structure approach, one-equation models use SGS kinetic energy to predict the magnitude of the modeled SGS stresses, and use normalized tensor terms to determine the SGS stress structure [42, 43]. For example, in SCDSM, $\tau_{ij} \approx 2k_{\text{sgs}}(\frac{\gamma_{ij}^M}{\gamma_{mm}^M})$. The SCDSM gives very high regression coefficients, $\beta > 0.9$, over all filter sizes in all directions (figure 16(a)). The other dynamic structure models, GCDSM and DSM, have similar results. This suggests that such models may be applicable for LES of a high Reynolds number isotropic turbulence using relatively coarse grids.

For rotating turbulence, as shown in the previous section (figures 15(d) and 16(b)), the correlation and the regression coefficients in the z -direction decrease much more rapidly with filter size than the other coefficients. Hence, to show the benefits of the new models, we compare the stress in the z -direction (τ_{33}) and the vector component in the z -direction ($\partial\tau_{3j}/\partial x_j$).

Figure 17 shows the z -direction regression coefficients for the new models. When compared to the SSM, three dynamic structure models have significantly higher regression coefficients

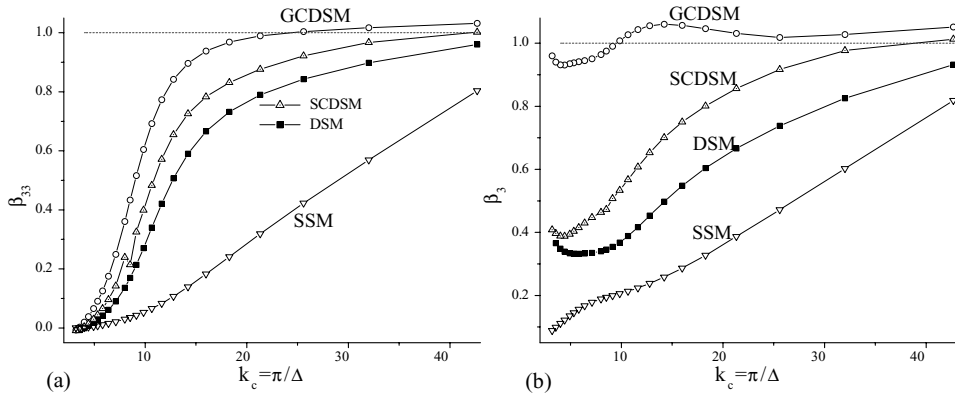


Figure 17. Regression coefficient for rotating case B5: (a) β_{33} and (b) β_3 .

in isotropic turbulence and noticeably better results in rotating turbulence. This is primarily due to the use of SGS kinetic energy to determine the magnitude of the SGS stresses.

In rotating turbulence, the two MFI-consistent models (GCDSM and SCDSM) show better results than the basic dynamic structure model (DSM). Maintaining material frame indifference in the model, either inherently or by construction, helps to diminish the problems of anisotropy that occur in rotating systems. Figure 17 shows that the GCDSM has some of the best results. For rotating turbulence, the GCDSM regression coefficient remains near 1 for all filter sizes. It gives $\beta > 0.8$ when $k_c > 13$ for τ_{33} , $\beta \approx 1$ for other stress terms, and nearly unit regression for vector components even when the grid is very coarsened. Note that at small filter sizes, the GCDSM does not approach the actual SGS stresses because the model is based on the first term in a Taylor series. This shortcoming is probably not significant in applications where coarser than DNS grids are used, especially given the generally very good results of this model.

All of the results presented here use the Gaussian filter in a discrete manner in physical space. We have explored the cut-off, the top-hat and the triangle filter [41, 42, 44]. The results are essentially the same as for the Gaussian filter. The primary difference was found with the cut-off filter which introduces additional physical space oscillations and can result in lower correlation coefficients. This is consistent with results presented by Liu et al. [30].

5.4 Energy production at subgrid scales

Kinetic energy transfer between resolved and subgrid scales occurs through the production term (also called the energy flux) that appears in the SGS kinetic energy equation. The term is defined as $P = -\tau_{ij}\bar{S}_{ij} = -\tau_{ij}\frac{\partial \bar{u}_i}{\partial x_j}$, and is useful for comparing various SGS stress models as shown in figures 18, 19 and 20.

For the isotropic case A, figure 18(a) shows that two eddy-viscosity models (SM and KEM) give correlation values of about 0.75 over a wide filter size range. This is a reasonably good correlation and illustrates why these models can predict global dissipation fairly accurately. For the rotating case B5, however, the eddy-viscosity models give correlations less than 0.05 (figure 18(b)). This indicates that in rotating systems these models will have trouble predicting even the total, global energy dissipation. High correlation coefficients above 0.8 can be obtained by other examined models in both cases. Figure 18 includes correlation results of the GCDSM and the SCDSM. Similarity-type models (e.g. SSM, DSM and SCDSM) have

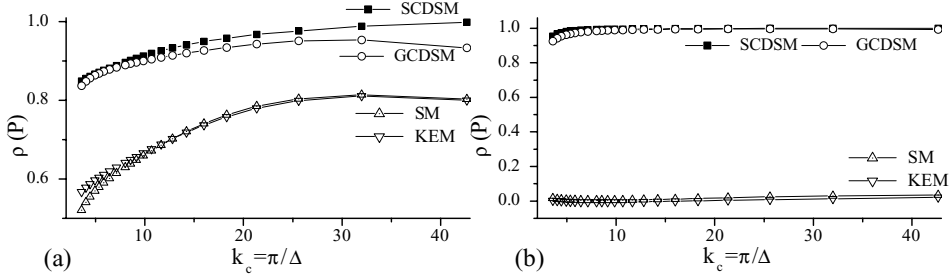


Figure 18. Correlation coefficients of production: (a) isotropic case A; (b) rotating case B5.

very similar correlation results, and also correlation values of gradient-type models (e.g. GM and GCDSM) are in very good agreement.

Examining the regression coefficient (figure 19) shows that the dynamic structure models (e.g. GCDSM and SCDSM) have much better results than the zero-equation high-correlation models (e.g. SSM and GM). The SSM and the GM significantly under estimate the magnitude of the energy production at larger filter sizes. This under-prediction of energy transfer is consistent with these models having more problems with stability when modeling high Reynolds number turbulence [1, 2].

In figure 20, we examine the power spectra of the energy transfer term at a given filter size for the rotating case B5. The SM is re-calculated by $(\frac{\tau_{ik}}{3}\delta_{ij} - 2\nu_t\bar{S}_{ij})$ to perform this comparison. Most of the models show spectra that monotonically increase from large-to-small scales, similar to the DNS spectra. The SSM and the GM show slightly lower values and the dynamic structure models show values close to or slightly higher than the DNS results, all consistent with figure 19 showing $\beta \approx 1$. However, figure 20 reveals significant inaccuracies in both the SM and the KEM. The SM is too dissipative at all scales and the KEM has the opposite trend from the DNS spectra. These results are consistent with figures 18 and 19 but reveal more details about the model behavior, particularly the KEM.

6. Preliminary *a posteriori* results

There could exist certain risks if a systematical investigation of the model performance in actual LES of turbulent flows had not been performed. For instance, the SSM gives superior results to the SM when tested at *a priori* level. However, the SSM alone does not dissipate enough energy at small scales and typically leads to inaccurate results [1]. Thus, a viscosity

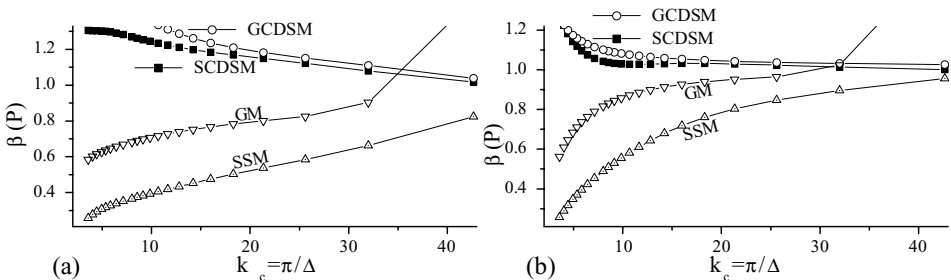


Figure 19. Regression coefficients of production: (a) isotropic case A; (b) rotating case B5.

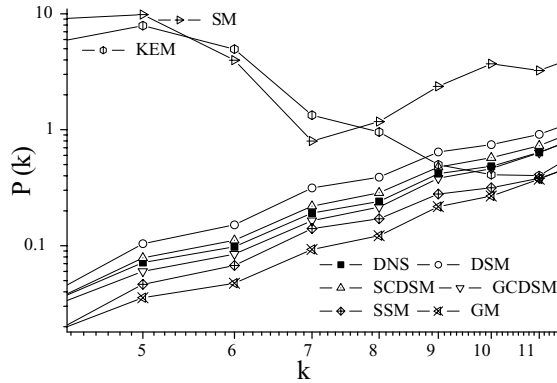


Figure 20. Power spectra of production for rotating case B5 (Gaussian filter at $k_c = 11$).

term has been added to the SSM resulting in a mixed version [1, 59]. In simulations of rotating turbulence, we are using a linear combination of new models and a hyper-viscosity term [17]

$$\text{MixGCDSM} : \tau_{ij} \approx \left(\frac{G_{ij}}{G_{mm}} \right) 2k_{\text{sgs}} + \nu_4 \nabla^2 \bar{S}_{ij} \quad (27)$$

$$\text{MixSCDSM} : \tau_{ij} \approx \left(\frac{\Upsilon_{ij}}{\Upsilon_{mm}} \right) 2k_{\text{sgs}} + \nu_4 \nabla^2 \bar{S}_{ij}, \quad (28)$$

where hyper-viscosity ν_4 can be modeled as $\nu_4 = C'_k \Delta^3 \sqrt{k_{\text{sgs}}}$, which is $O(\Delta^4)$, and can be treated as a model of the second term of the Taylor expansion of SGS stress (3). It must be noted that typically the magnitude of the structure term (e.g. the similarity term, and the gradient term) is significantly higher than that of the viscosity term (≈ 50 when measured in the L_2 -norm), and comparing with the scatter plot 11 for the similarity term, the viscosity term is much more isotropically distributed (as a consequence, the viscosity term gives much lower correlation). Hence, the viscosity term does not degrade the *a priori* results [31].

We have assessed SGS models including the dynamic smagorinsky model (DynSM, [19, 29]), and compared with the DNS results for incompressible isotropic and rotating turbulences. Figure 21 shows the temporal variations of the resolved kinetic energy for a decaying isotropic

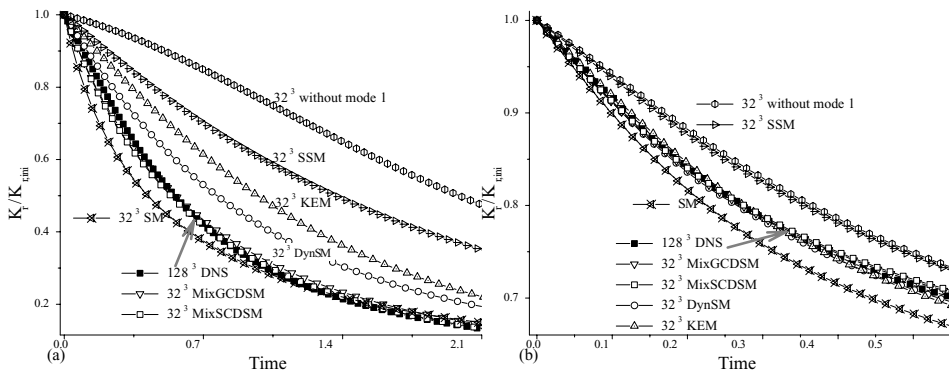


Figure 21. Evolution of resolved kinetic energy, time is normalized by initial eddy turn-over time: (a) decaying isotropic turbulence, initially $\text{Re}_\lambda = 85$; (b) decaying rotating turbulence, initially $\text{Re}_\lambda = 86$, $\text{Ro}^{\omega 3} = 0.41$, and $\text{Ro}^L = 0.025$.

turbulence case (initial $\text{Re}_\lambda = 85$) and a decaying rotating turbulence ($\Omega = 1.0$ (rad s⁻¹), initial $\text{Re}_\lambda = 86$, $\text{Ro}^{\omega_3} = 0.41$, and $\text{Ro}^L = 0.025$). In both cases, the results obtained using the MixGCDSM and the MixSCDSM yield better agreement with the filtered DNS data than other SGS models. More specific details and *a posteriori* results will be included in the coming paper.

7. Summary and conclusions

The current work has used *a priori* tests to investigate the performance of a variety of SGS models in rotating turbulent flows. Many models were examined and compared using correlation and regression coefficients, from traditional eddy-viscosity models to new one-equation models introduced herein.

As is well known, eddy-viscosity models (e.g. SM and KEM) are purely dissipative, and analysis of the SGS energy production showed that the SM and the KEM are too dissipative at all scales in rotating turbulence. This is not surprising since eddy-viscosity models were originally conceived for isotropic turbulence, and it is also well known that strong rotating inhibits the forward cascade of energy leading to lower levels of the energy dissipation rate. In addition, eddy-viscosity models failed to give good correlation coefficients in both isotropic and rotating turbulence, and these coefficients were lower for rotating turbulence.

Most classical SGS models, including eddy-viscosity models and the scale similarity model have no explicit method to account for anisotropy of length scales and material frame indifference of the SGS stress tensor, and thus they perform poorly in rotating turbulence. We examined additional models (the KEM and the DSM) that showed somewhat better results, but still do not satisfy the consistency with MFI at the stress tensor level, and therefore failed to capture the anisotropy effects due to rotation.

To account properly for MFI, we introduced two new one-equation models which are variants of the dynamic structure model, namely the GCDSM and the SCDSM. By construction these new models satisfy the consistency with MFI and the trace requirement $\tau_{ii}^{\text{model}} = 2k_{\text{sgs}}$. Accordingly these new models greatly improve the regression coefficients for modeling components in all directions. The evaluation of model performance in this comparative study of various SGS models is summarized in table 2. The models are listed with symbols to indicate if they performed poorly, well, or very well on each diagnostic.

In this research, DNS validation cases were performed at a moderate Reynolds number for forced isotropic turbulence and moderate Rossby numbers for forced rotating turbulence

Table 2. Comparison of model performance in LES of rotating turbulence at the *a priori* test level

Diagnostic	SM	KEM	SSM	GM	DSM	SCDSM	GCDSM
ρ_{ij}	–	*	+	+	+	+	+
$\beta_{ij}, (i, j \neq 3)$	–	*	+	+	+	++	++
β_{3j}	–	–	–	–	–	+	++
ρ_i	–	–	+	+	+	+	+
$\beta_i, (i \neq 3)$	–	–	+	+	+	++	++
β_3	–	–	–	+	–	+	++
$\rho(P)$	–	–	+	+	+	+	+
$\beta(P)$	–	–	–	–	+	++	++

The symbols –, + and ++ refer to bad, good and very good results.

*Good on $\rho_{11}, \rho_{22}, \beta_{11}$ and β_{22} , but bad on cross terms, $\rho_{i,(i \neq j)}$ and $\beta_{i,(i \neq j)}$.

consistent with the grid resolution used. Details of the comparison may be valid only for those cases, but some studies are expected to be more generally applicable, such as the regression coefficient analysis, the invariance of SGS models and the influence of anisotropy on LES modeling. Nevertheless, there exists a need of *a posteriori* tests in rotating turbulence. Also, it is important to study more complex flows (e.g. rotating stratified turbulence and channel flow subject to system rotation), which are physically realizable and admit a quantitative comparison with experimental results.

Acknowledgement

This material is based upon work supported by the National Science Foundation (NSF) under grant no. 0500056 and by the NSF Scientific Computing Research Environments in the Mathematical Sciences (SCREMS) under grant no. DMS-0532085. We would like to thank Dr. Yun-Liang Wang for useful discussions and the Engine Research Center at the University of Wisconsin - Madison for providing computing resources.

Appendix. *a priori* tests of other rotating cases

Although the *a priori* analysis was carried out on all the DNS data sets, only case B5 was discussed in the primary paper. Here, we present other examples to demonstrate the consistency of the conclusions.

A.1 Tests of another 128^3 hyper-viscosity rotating case

In case B5, we input energy using the Gaussian white-noise forcing scheme at small scales ($k_f = 21$). In case C3, we input energy using the same scheme at large scales ($k_f = 2.5$). Hypo- and hyper-viscosities were used in both computations to produce a reasonable inertial range and stationary results. More importantly, two cases have some differences in the underlying physical processes (figures 5–8). For example, in case B5, the reverse energy transfer from small-to-large scales is the only energy source for the flow at large scales. The 3D and 2D spectrum plots 6 and 7 show that the flow at large scales is more two-dimensionalized when forced at small scales than when forced at large scales.

However, two cases have the similar regression coefficient results in two aspects: (i) there exists an overall tendency that the regression coefficient decreases when the filter size increases, and also the z -direction regression coefficients decrease much more rapidly (not plotted here); (ii) as shown in figures A1 and 17, the two MFI-consistent one-equation models (GCDSM and SCDSM) have higher regression coefficients than the others, and the GCDSM has some of the best results. We have consistent conclusions for energy production term which are not plotted here.

A.2 Tests of a 256^3 real-viscosity rotating case

We have performed *a priori* tests of a 256^3 real-viscosity rotating turbulent case, which has reached its quasi-steady state with $Re_\lambda = 180$. Figure A2 shows the 3D and 2D energy spectra of this case. In order to compare with the results of 128^3 large-scale forced hyper-viscosity runs (C series), we have chosen the same Gaussian forcing peak wave number $k_f = 2.5$, and have matched Rossby number $Ro^G = 0.12$.

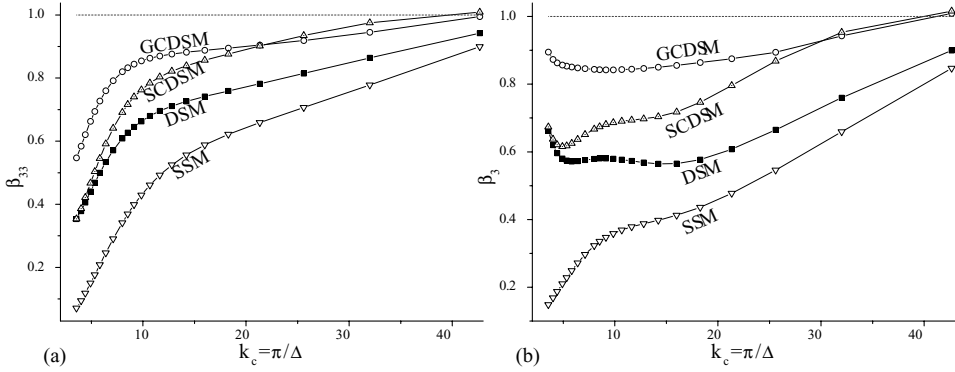


Figure A1. Regression coefficients for large scale forced rotating case C3: (a) β_{33} and (b) β_3 .

The 256^3 case allows us to do correlation–regression studies up to $k_c = 85$. Figure A3 compares the regressions for 128^3 hyper-viscosity rotating case C3 and 256^3 real-viscosity rotating case. Clearly, the overall tendency that the regression coefficient decreases when the filter size increases is observed. Figure A3 shows that dynamic structure models (DSM, GCDSM and SCDSM) have an advantage over the SSM in giving more accurate modeling of SGS stress, also the two MFI-consistent one-equation models (GCDSM and SCDSM) seem very promising to give higher regressions compared to other models.

In the primary paper, we adopt hyper-viscosity approach to shorten the dissipative range [5, 6]. It enables us to focus on the inertial range to study the behaviors of SGS models. As shown in figure A3, the regression coefficients decrease more rapidly in the 128^3 hyper-viscosity case when the filter size increases. The advantages of MFI-consistent dynamic structure models can be more markedly illustrated.

It is important to note that all rotating cases in the present study have the same Taylor micro-scale features (e.g. inequalities (15)). As discussed in sections 5.3.2 and 5.3.3, a large-size filtering, which can be characterized by a normalized filter size (e.g. the ratio of filter size to micro-scale), compresses the small-scale turbulence and lowers the correlation and the regression coefficients overall. Because $\lambda_{f,3}$ is smaller than the others, a relative coarser filtering was employed in the z -direction. It results in the regression coefficients decrease

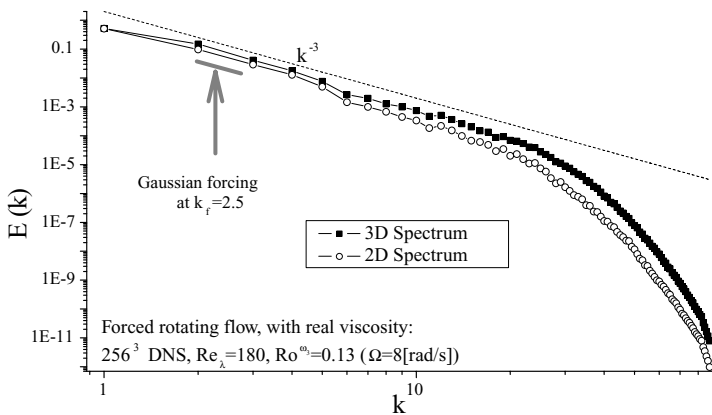


Figure A2. Energy spectrum of a 256^3 large scale forced real-viscosity rotating turbulence.

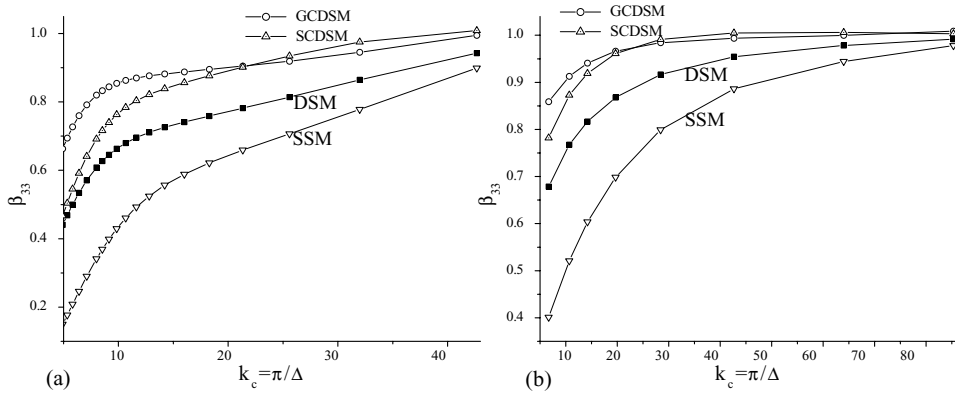


Figure A3. Regression coefficients for τ_{33} : (a) in 128^3 large-scale forced hyper-viscosity rotating case C3, and (b) in 256^3 large-scale forced real-viscosity rotating case.

much more rapidly in the z -direction, especially for those inconsistent SGS models who assume that the small scale turbulence is nearly isotropic and do not account for rotational effects (e.g. SSM and DSM). The consistency with the constraint of MFI is a theoretical standpoint concerning turbulent constitutive relation for SGS stress in a non-inertial frame of reference undergoing rotation. This comparative study has successfully revealed that the new MFI-consistent one-equation models achieve better regression coefficient values in all directions.

References

- [1] Bardina, J., Ferziger, J.H. and Reynolds, W.C., 1980, Improved subgrid scale models for large eddy simulation. *AIAA Paper 80-1357*.
- [2] Bardina, J., Ferziger, J.H. and Reynolds, W.C., 1983, Improved turbulence models based on large eddy simulation of homogeneous incompressible, turbulent flows. *Technical Report No. TF-19*, Thermosciences Division, Department of Mechanical Engineering, Stanford University, Stanford, California.
- [3] Bardina, J., Ferziger, J.H. and Rogallo, R.S., 1985, Effect of rotation on isotropic turbulence: computation and modeling. *Journal of Fluid Mechanics*, **154**, 321–336.
- [4] Bartello, P., Metais, O. and Lesieur, M., 1994, Coherent structures in rotating three-dimensional turbulence. *Journal of Fluid Mechanics*, **273**, 1–29.
- [5] Borue, V., 1994, Inverse energy cascade in stationary two-dimensional homogeneous turbulence. *Physical Review Letters*, **72**(10), 1475–1478.
- [6] Borue, V. and Orszag, S.A., 1995, Self-similar decay of three-dimensional homogeneous turbulence with hyperviscosity. *Physical Review E*, **51**(2), R856–R859.
- [7] Borue, V. and Orszag, S.A., 1996, Numerical study of three-dimensional Kolmogorov flow at high Reynolds numbers. *Journal of Fluid Mechanics*, **306**, 293–323.
- [8] Cambon, C., Mansour, N.N. and Godeferd, F.S., 1997, Energy transfer in rotating turbulence. *Journal of Fluid Mechanics*, **337**, 303–332.
- [9] Cambon, C., Mansour, N.N. and Squires, K.D., 1994, Anisotropic structure of homogeneous turbulence subjected to uniform rotation. *Proceeding of the Summer Program*, pp. 397–420.
- [10] Canuto, C., Hussaini, M.Y., Quarteroni, A. and Zang, T.A., 1988, *Spectral Methods in Fluid Dynamics* (Berlin: Springer).
- [11] Chasnov, J.R., 1994, Similarity states of passive scalar transport in isotropic turbulence. *Physics of Fluids*, **6**(2), 1036–1051.
- [12] Chumakov, S.G. and Rutland, C.J., 2004, Dynamic structure models for scalar flux and dissipation in large eddy simulation. *AIAA Journal*, **42**(6), 1132–1139.
- [13] Chumakov, S.G. and Rutland, C.J., 2005, Dynamic structure subgrid-scale models for large eddy simulation. *International Journal for Numerical Methods in Fluids*, **47**, 911–923.
- [14] Clark, R.A., Ferziger, J.H. and Reynolds, W.C., 1979, Evaluation of subgrid-scale models using an accurately simulated turbulent flow. *Journal of Fluid Mechanics*, **91**(1), 1–16.
- [15] Cook, A.W., 1997, Determination of the constant coefficient in scale similarity models of turbulence. *Physics of Fluids*, **9**(5), 1485–1487.

- [16] Deardorff, J.W., 1973, The use of subgrid transport equations in a three-dimensional model of atmospheric turbulence. *Journal of Fluid Engineering*, **95**, 429–438.
- [17] Ferziger, J.H., 2000, *Large Eddy Simulation—A Short Course*. (Stanford, CA: Stanford University)
- [18] Germano, M., 1986, A proposal for a redefinition of the turbulent stresses in the filtered Navier–Stokes equations. *Physics of Fluids*, **29**(7), 2323–2324.
- [19] Germano, M., Piomelli, U. and Cabot, W.H., 1991, A dynamic subgrid-scale eddy viscosity model. *Physics of Fluids A*, **3**(7), 1760–1765.
- [20] Geurts, B.J., 2001, *Modern simulation strategies for turbulent flow*. (Philadelphia, PA: R. T. Edwards, Inc.).
- [21] Horiuti, K., 1993, A proper velocity scale for modeling subgrid-scale eddy viscosities in large eddy simulation. *Physics of Fluids A*, **5**(1), 146–157.
- [22] Horiuti, K., 1997, A new dynamic two-parameter mixed model for large-eddy simulation. *Physics of Fluids*, **9**(11), 3443–3464.
- [23] Horiuti, K., 2001, Rotational transformation and geometrical correlation of SGS models. In: B.J. Geurts, editor *Modern Simulation Strategies for Turbulent Flow*, pages 123–140. (Philadelphia, PA: R.T. Edwards Inc.)
- [24] Horiuti, K., 2006, Transformation properties of dynamic subgrid-scale models in a frame of reference undergoing rotation. *Journal of Turbulence*, **7**(16):1–27.
- [25] Kim, W.-W. and Menon, S., 1995, A new dynamic one-equation subgrid-scale model for large eddy simulations. *AIAA-1995-356, Aerospace Sciences Meeting and Exhibit, 33rd, Reno, NV*.
- [26] Kobayashi, H. and Shimomura, Y., 2001, The performance of dynamic subgrid-scale models in the large eddy simulation of rotating homogeneous turbulence. *Physics of Fluids*, **13**(8), 2350–2360.
- [27] Leonard, A., 1974, Energy cascade in large-eddy simulation of turbulent fluid flows. *Advances in Geophysics*, **18**, 237.
- [28] Lilly, D.K., 1983, Stratified turbulence and the mesoscale variability of the atmosphere. *Journal of Atmospheric Sciences*, **40**, 749–761.
- [29] Lilly, D.K., 1992, A proposed modification of the Germano subgrid-scale closure method. *Physics of Fluids*, **4**(3), 633–635.
- [30] Liu, S., Meneveau, C. and Katz, J., 1994, On the properties of similarity subgrid-scale models as deduced from measurements in a turbulent jet. *Journal of Fluid Mechanics*, **275**, 83–119.
- [31] Liu, S., Meneveau, C. and Katz, J., 1995, Experimental study of similarity subgrid-scale models of turbulence in the far-field of a jet. *Applied Scientific Research*, **54**, 177–190.
- [32] Lumley, J.L., 1970, Toward a turbulent constitutive relation. *Journal of Fluid Mechanics*, **41**(2), 413–434.
- [33] Mansour, N.N., Cambon, C. and Speziale, C.G., 1992, Studies in turbulence. In: *Theoretical and Computational Study of Rotating Isotropic Turbulence* edited by T. B. Gatski and S. Sarkar and C. G. Speziale (New York: Springer).
- [34] McMillan, O.J., Ferziger, J.H. and Rogallo, R.S., 1980, Tests of new subgrid scale models in strained turbulence. *AIAA Paper 80-1339*.
- [35] Menon, S., Yeung, P.-K. and Kim, W.-W., 1996, Effect of subgrid models on the computed interscale energy transfer in isotropic turbulence. *Computers and Fluids*, **25**(2), 165–180.
- [36] Morinishi, Y., Nakabayashi, K. and Ren, S.Q., 2001, Dynamic of anisotropy on decaying homogeneous turbulence subjected to system rotation. *Physics of Fluids*, **13**(10), 2912–2922.
- [37] Morinishi, Y., Nakabayashi, K. and Ren, S.Q., 2001, A new DNS algorithm for rotating homogeneous decaying turbulence. *International Journal of Heat and Fluid Flow*, **22**, 30–38.
- [38] Overholt, M.R. and Pope, S.B., 1998, A deterministic forcing scheme for direct numerical simulations of turbulence. *Computers and Fluids*, **27**(1), 11–28.
- [39] Pedlosky, J., 1986, *Geophysical Fluid Dynamics*. (New York: Springer)
- [40] Piomelli, U. and Liu, J., 1995, Large-eddy simulation of rotating channel flows using a localized dynamic model. *Physics of Fluids*, **7**(4), 839–848.
- [41] Piomelli, U., Moin, P. and Ferziger, J.H., 1988, Model consistency in large eddy simulation of turbulent channel flows. *Physics of Fluids*, **31**(7), 1884–1891.
- [42] Pomraning, E., 2000, Development of large eddy simulation turbulence models. *PhD thesis*, University of Wisconsin, Madison.
- [43] Pomraning, E. and Rutland, C.J., 2002, Dynamic one-equation nonviscosity large-eddy simulation model. *AIAA Journal*, **40**, 689–701.
- [44] Pope, S.B., 2000, *Turbulent Flows*. (Cambridge: Cambridge University Press).
- [45] Segel, L.A., 1977, *Mathematics Applied to Continuum Mechanics*. (New York: Macmillan)
- [46] Shimomura, Y., 1999, A family of dynamic subgrid-scale models consistent with asymptotic material frame indifference. *Journal of the Physical Society of Japan*, **68**(8), 2483–2486.
- [47] Smagorinsky, J., 1963, General circulation experiments with the primitive equations: I. The basic experiment. *Monthly Weather Review*, **91**(3), 99–164.
- [48] Smith, L.M., Chasnov, J.R. and Waleffe, F., 1996, Crossover from two- to three-dimensional turbulence. *Physical Review Letters*, **77**(12), 2467–2470.
- [49] Smith, L.M. and Lee, Y., 2005, On near resonances and symmetry breaking in forced rotating flows at moderate Rossby number. *Journal of Fluid Mechanics*, **535**, 111–142.
- [50] Smith, L.M. and Waleffe, F., 1999, Transfer of energy to two-dimensional large scales in forced, rotating three-dimensional turbulence. *Physics of Fluids*, **11**(6), 1608–1622.

- [51] Smith, L.M. and Waleffe, F., 2002, Generation of slow large scales in forced rotating stratified turbulence. *Journal of Fluid Mechanics*, **451**, 145–168.
- [52] Speziale, C.G., 1983, Closure models for rotating two-dimensional turbulence. *Geophysical and Astrophysical Fluid Dynamics*, **23**, 69–84.
- [53] Speziale, C.G., 1985, Galilean invariance of subgrid-scale stress models in the large-eddy simulation of turbulence. *Journal of Fluid Mechanics*, **156**, 55–62.
- [54] Speziale, C.G., 1985, Subgrid scale stress models for the large-eddy simulation of rotating turbulent flows. *Geophys. Astrophys. Fluid Dynamics*, **33**, 199–222.
- [55] Speziale, C.G., 1989, Turbulence modeling in non-inertial frames of reference. *Theoretical and Computational Fluid Dynamics*, **1**(3).
- [56] Taylor, G.I., 1935, Statistical theory of turbulence. *Proceedings of the Royal Society of London. Series A, Mathematical and Physical Sciences*, **151**(873), 421–444.
- [57] Yeung, P.K. and Zhou, Y., 1998, Numerical study of rotating turbulence with external forcing. *Physics of Fluids*, **10**(11), 2895–2909.
- [58] Yoshizawa, A. and Horiuti, K., 1985, A statistically-derived subgrid-scale kinetic energy model for the large-eddy simulation of turbulent flows. *Journal of the Physical Society of Japan*, **54**(8), 2834–2839.
- [59] Zang, Y., Street, R.L. and Koseff, J.R., 1993, A dynamic mixed subgrid-scale model and its application to turbulent recirculating flows. *Physics of Fluids A*, **5**(12), 3186–3196.